Nickel-Oxide-Modified SrTiO₃(110)-(4 × 1) Surfaces and Their Interaction with Water

Stefan Gerhold,*,[†] Michele Riva,[†,‡] Zhiming Wang,[†,§] Roland Bliem,[†] Margareta Wagner,[†] Jacek Osiecki,[∥] Karina Schulte,[∥] Michael Schmid,[†] and Ulrike Diebold*,[†]

[†]Institute of Applied Physics, TU Wien, Wiedner Hauptstraße 8-10, 1040 Vienna, Austria

[‡]CNISM - Dipartimento di Fisica, Politecnico di Milano, Piazza Leonardo da Vinci 32, I-20133 Milano, Italy

[§]Swiss Light Source, Paul Scherrer Institute, 5234 Villigen, Switzerland

[∥]MAX IV Laboratory, Lund University, Ole Römers väg 1, 223 63 Lund, Sweden

ABSTRACT: Nickel oxide (NiO), deposited onto the strontium titanate (SrTiO₃) (110)-(4 × 1) surface, was studied using photoemission spectroscopy (PES), X-ray absorption near edge structure (XANES), and low-energy He⁺ ion scattering (LEIS), as well as scanning tunneling microscopy (STM). The main motivation for studying this system comes from the prominent role it plays in photocatalysis. The (4 × 1) reconstructed SrTiO₃(110) surface was previously found to be remarkably inert toward water adsorption under ultrahigh-vacuum conditions. Nickel oxide grows on this surface as patches without any apparent ordered structure. PES and LEIS reveal an upward band bending, a reduction of the band gap, and reactivity toward water adsorption upon deposition of NiO. Spectroscopic results are discussed with respect to the enhanced reactivity toward water of the NiO-loaded surface.
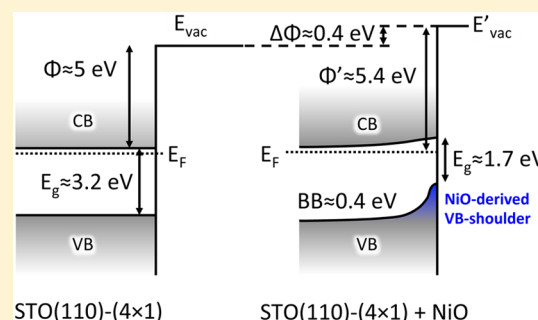
INTRODUCTION

Strontium titanate (SrTiO₃, STO), the prototypical perovskite oxide, has long been known to show interesting effects taking place on its surfaces. For example, it is commonly used as a substrate for the growth of complex oxides,[1] and it supports the formation of a two-dimensional electron gas on its surfaces.[2,3] Furthermore, SrTiO₃ was one of the first materials to show a higher photocatalytic water-splitting efficiency[4] than the classical photocatalyst TiO₂.[5]

What makes a material a good photocatalyst are an appropriate band gap allowing harvesting most of the solar spectrum (maximum intensity at around 2.4 eV) and a suitable alignment of the valence band maximum (VBM) and conduction band minimum (CBM) with respect to the redox potentials of water. As was found by Scaife,[6] for most semiconducting transition metal oxides, the (H₂O/H₂) redox potential of water lies around 3 V above the VBM, i.e., inside the band gap for SrTiO₃ (E_g = 3.2 eV). This means that band engineering toward an efficient photocatalyst should decrease the magnitude of the band gap while retaining the position of the CBM.

Such band engineering was already successfully demonstrated by Konta et al. by doping STO with rhodium.[7] The rhodium dopants introduce an impurity level located 2.3 eV below the CBM of STO. Visible light can therefore excite electrons from the dopant levels into the conduction band of STO, and the photocatalytic process is initiated.

Recently, we have studied the adsorption of water on the pristine SrTiO₃(110)-(4 × 1) surface.[8] This reconstruction is formed to compensate for the polarity of the STO(110) surface.[9,10] The structure consists of six- and ten-membered rings of TiO₄ tetrahedra, sitting on a bulk-truncated STO(110) plane, in which titanium is octahedrally coordinated. We found that this surface is remarkably inert toward the interaction with water, providing a very good starting point for studying the effect of promoters.[8]

The photocatalytic activity of the SrTiO₃:NiO system has already been demonstrated successfully by Townsend and co-workers.[11] In their study, Townsend et al. showed that "NiOₓ-STO is more likely a three-component Ni-STO-NiO catalyst, in which STO absorbs the light, Ni reduces protons, and NiO oxidizes water". The present study is intended to provide fundamental information on the SrTiO₃:NiO system. We have performed X-ray absorption near-edge structure (XANES), X-ray and ultraviolet photoelectron spectroscopy (XPS/UPS), and scanning tunneling microscopy (STM) to determine the effects of adsorption of NiO onto the STO(110)-(4 × 1) surface. NiO was prepared by either (i) postoxidation of submonolayer amounts of Ni deposited by molecular beam epitaxy (MBE) in ultrahigh vacuum or (ii) reactive MBE growth of metallic Ni in a molecular oxygen background. STM

reveals that the nanometer-sized NiO patches that develop on STO(110)-(4 × 1) distort the local surface structure independently of the preparation method. Consistently, XANES indicates a distortion/transformation of the surface TiO_4 tetrahedra upon NiO growth. Band bending is observed in both XPS and UPS, which increases with the amount of NiO. The onset of the VBM is effectively shifted upward, while minimal changes are observed on the CBM, as seen in the XANES results. Combining XPS, UPS, and low-energy ion scattering spectroscopy (LEIS), a clear signature of dissociative adsorption of water is found.

■ MATERIALS AND METHODS

Nb-doped (0.5 wt %) $SrTiO_3$ single crystals with polished (110) surface were purchased from MaTecK (Germany) and CrysTec (Germany). The STO(110)-(4 × 1) surface was prepared by cycles of sputtering (Ar^+, 1 keV, 5 μA, 10 min) and annealing (900 °C, 3×10^{-6} mbar O_2, 1 h). The samples were heated either by passing alternating current (7.6 V, 1.75 A) through the samples or by bombarding them with electrons from the back (900 V, 15 mA). Sample temperatures were measured with an infrared pyrometer (emissivity of 0.8). The STO(110) surface exhibits a series of well-defined reconstructions, which can be tuned by the Sr/Ti stoichiometry in the near-surface region.[12] For the present investigation the surface structure was adjusted to yield the 4 × 1 reconstruction,[9] as checked by low-energy electron diffraction (LEED). Nickel metal (purity of 99.999%) was deposited onto the surface from an electron beam evaporator (Omicron EFM3), with a typical growth rate of 0.1 Å/min, as measured in UHV via a home-built quartz-crystal microbalance. The oxidation of metallic Ni was achieved either by reactively depositing (RD) Ni in 5×10^{-6} mbar of O_2 at different temperatures (room temperature [RT], <300 °C, and 355 °C) or by postoxidizing (PO) the submonolayer Ni amounts (deposited in ultrahigh vacuum at RT) in 5×10^{-6} mbar of O_2 for 20 min. In the latter case, the substrate temperature was adjusted to be slightly below the onset of the IR pyrometer reading (300 °C), unless otherwise stated. In the following, all stated thicknesses refer to the deposited amount of metallic Ni. Synchrotron radiation photoemission spectroscopy (PES) and X-ray absorption spectroscopy (XANES) experiments were performed at beamline I311 at the MAX-lab laboratory.[13] The base pressure of the beamline end station was below 1×10^{-10} mbar. All synchrotron-based photoemission spectra (SCIENTA SES200 analyzer) were acquired with a takeoff angle for the photoelectrons of approximately 55° away from the surface normal and with suitable kinetic energies (see spectra for photon energies) to ensure highest surface sensitivity. Only one set of photon energy measurements was carried out for each sample treatment by measuring the Fermi-edge position on the Ta sample holder. Therefore, uncertainties of binding energies are stated for the shown synchrotron-based spectra. Work functions (Φ) were determined from a straight line tangent to the leading edge of the low kinetic-energy cutoff of the secondary electrons, as measured at normal emission with a sample bias of −10 V. X-ray absorption was performed in two different modes. Auger-electron yield (AEY) spectra were acquired by measuring the intensity of the Ti $L_2M_{2,3}M_{2,3}$ Auger peak, while sweeping the photon energy across the Ti $L_{2,3}$ edge. In secondary-electron yield (SEY), the increase of low-kinetic-energy electrons ($E_{kin} \approx 60$ eV) was measured as an indication of the absorption of X-rays. STM experiments were performed

in a separate UHV system with a SPECS Aarhus STM at room temperature (RT), using electrochemically etched W tips. All STM images were taken in constant-current mode with approximately +2 V sample bias voltage (empty states) and a tunneling current of around 0.2 nA. XPS (Omicron X-ray source with Al anode, $h\nu$ = 1486.7 eV) and LEIS (SPECS IQ12/38, 1000 eV He^+ ions, $\sim 5.8 \times 10^{11}$ $He^+/[cm^2 \, s]$, and total scattering angle $\theta = 127°$) experiments were performed with a SPECS Phoibos 100 hemispherical analyzer in the same analysis chamber with a base pressure below 6×10^{-11} mbar. Because of the small uncertainties in the photon energy calibration for the experiments performed at Max-lab synchrotron radiation facility, measurements of band bending as a result of different surface treatments were repeated in the home laboratory, providing a well-defined photon energy. Such band bending was derived from the binding energy of fitted XPS core-levels (O 1s and Ti $2p_{3/2}$). Samples were prepared in a connected preparation chamber with a base pressure of 3×10^{-10} mbar. Deionized water and isotopically labeled $H_2^{18}O$ (Sigma-Aldrich) were cleaned by repeated freeze−pump−thaw cycles and dosed onto the sample in the preparation chambers through high-precision leak valves. Peaks in ion scattering spectra have been assigned by calculating the kinetic energy of He^+ ions elastically scattered by ^{16}O, ^{18}O, Ti, Ni, and Sr atoms, considering a 127° total scattering angle.

■ RESULTS

Figure 1a shows photoemission spectra (raw data) of the valence band region of differently treated $SrTiO_3$(110)-(4 × 1) surfaces. The inset shows a zoom into the gap region with the spectra aligned at the O 2s peak at $E_B \approx 22$ eV (not shown). VBM were determined from the intersection of the horizontal (zero counts) line with a straight segment tangent to the leading edge of the UPS spectra, as represented in the inset of Figure 1a. For the clean surface (black curve), the onset of the valence band is located at approximately 3.2 eV below the Fermi level, in nice agreement with the n-type doping of the STO crystals and a reported band gap of 3.2 eV,[14] i.e., a flat-band situation. The gap-region of the pristine surface does not show any detectable density of states, meaning that no in-gap states are introduced by the Nb dopants in the STO single crystal.

Evaporation of Ni (red curve) shifts all spectral features to lower binding energies (by 0.22 ± 0.15 eV) and an in-gap state is formed. The adsorption of single Ni adatoms at the $SrTiO_3$(110)-(4 × 1) surface has been studied recently,[15] showing that isolated Ni adatoms are formed up to a coverage of 0.05 Å [see Figure 2b].

Upon postoxidizing the Ni adatoms, the valence band shifts to even lower binding energies by 0.38 ± 0.15 eV compared to the pristine surface, and the in-gap state is shifted downward, forming a shoulder of the valence band. In the case of 0.1 Å Ni postoxidized, the onset of the valence band is shifted to lower binding energies by around 1.5 eV [inset of Figure 1a]. The upward bending of the energy bands as a result of NiO adsorption is consistent with the higher workfunction of NiO compared to the pristine STO surface ($\Phi_{STO(110)-(4\times1)} \approx 4.9$ eV, $\Phi_{NiO} = 6.2-6.7$ eV)[16] and the measured increase of the workfunction of the NiO-loaded surface ($\Phi_{STO+0.1\,ÅNiO} \approx 5.3$ eV).

Figure 1b shows the Ni 2p core-level spectra measured on as-deposited 0.1 Å Ni (red) and after postoxidizing the sample (blue). The as-deposited Ni exhibits the typical metallic Ni 2p
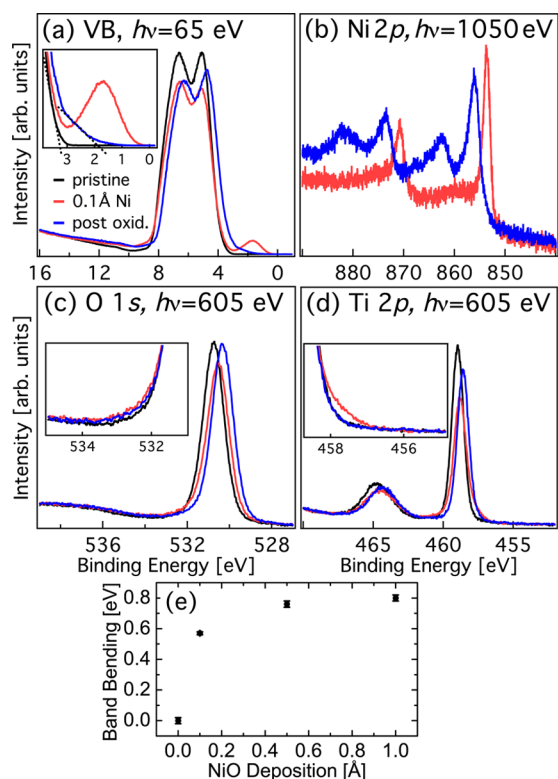
Figure 1. Photoemission spectra of differently treated SrTiO$_3$(110)-(4 × 1) surfaces. Black, red, and blue spectra correspond to the pristine surface, the surface after deposition of 0.1 Å Ni, and after postoxidizing the same Ni amount at 300 °C, respectively. (a) Valence band spectra. The inset shows a zoom into the gap region with the spectra aligned to the O 2s feature at 22 eV. Dotted lines are used to evaluate the onset of the valence band. (b) Ni 2p core levels before and after oxidizing 0.1 Å Ni. (c) O 1s and (d) Ti 2p core-level features. The insets show the O 1s high binding-energy region (c) and the Ti 2p$_{3/2}$ low binding-energy region (d) after aligning the spectra to the corresponding main peak. (e) Band bending as measured from the O 1s and Ti 2p peak positions with Al Kα radiation as a function of the RD-deposited NiO deposition amount (quartz crystal microbalance readings assuming Ni density; error bars represent 99% confidence intervals on the fitted peak positions).

core-level features with a binding energy of the j = 3/2 component of 853.6 ± 0.3 eV and a 17.1 eV spin−orbit-split (SOS) 2p$_{1/2}$ peak (compared to 2p$_{3/2}$ photoemission from pure metallic Ni at E_B = 852.7 eV with a SOS of 17.3 eV).[17] Upon postoxidizing the nickel, the Ni 2p core-level features change to the typical NiO line shape, with a binding energy of the j = 3/2 component of 855.9 ± 0.3 eV and a SOS of 17.6 eV (compared to literature values of E_B = 853.8 eV of 2p$_{3/2}$ and SOS = 17.5 eV for bulk NiO[17]).

The O 1s core-level [Figure 1c] shows only a very weak change. The presence of Ni adatoms causes the main O 1s spectral feature to be damped and a small shoulder at higher binding energy is formed. This shoulder is slightly diminished upon postoxidation [see inset of Figure 1c, in which the spectra are shifted for clarity, aligning the main O 1s feature]. The effect of nickel adatoms binding to the surface oxygen can also be seen in the Ti 2p core-level spectra in Figure 1d. Here, the pristine surface (black) shows the commonly observed Ti 2p features of Ti^{4+} ions (Ti 2p$_{3/2}$ E_B = 459 ± 0.15 eV with a SOS of 5.7 eV). Upon deposition of Ni adatoms, a shoulder at lower binding energies is formed, as it can be seen in the inset of

Figure 1d. Such a shoulder is normally assigned to reduced Ti^{3+} species, as described elsewhere.[18] Upon oxidation, this shoulder vanishes, and the spectrum resembles the pristine surface, except for a rigid shift of 0.2 ± 0.15 eV to lower BE. Band bending is found to progressively increase with the successive deposition of NiO, attaining a saturation value of approximately 0.8 eV at deposited amounts above 1 Å NiO [see Figure 1e].

The (4 × 1) reconstructed surface of SrTiO$_3$(110), having a unit cell size of 15.6 Å × 5.52 Å, appears in STM images as periodic double lines of weak maxima along the [1$\bar{1}$0] direction [see Figure 2a]. These maxima correspond to TiO$_4$ tetrahedra, which form six- and ten-membered rings via corner-sharing oxygen atoms.[9] Bright protrusions on the (4 × 1) rows [a few marked by green dots in Figure 2a] are assigned to single strontium adatoms, which are stabilized on antiphase domain boundaries of the reconstruction, ensuring polarity compensation.[19]

We have recently investigated the adsorption of nickel on this surface,[15] showing that isolated single Ni adatoms [red stars in Figure 2b] are stabilized when submonolayer Ni amounts are deposited on STO at RT. Ni adatoms can adsorb either at the center of (4 × 1) rows (six-membered TiO$_4$ rings) or on their sides, in proximity of the dark trenches (ten-membered TiO$_4$ rings).[15]

Upon postoxidizing 0.1 Å Ni in 5 × 10^{-6} mbar of O$_2$ at 375 °C, the Ni adatoms coalesce into irregularly shaped patches [highlighted by the dashed blue line in Figure 2c], extending over several adjacent (4 × 1) lines, and not showing any apparent preferential adsorption site. No clear ordering of atomic-scale features could be observed on such patches, likely indicating the formation of a locally defective NiO structure. Similar morphological and structural features are observed when growth is carried out by reactively depositing Ni in O$_2$ atmosphere [Figure 2d,e], and no significant improvement of the measurable atomic-scale structure is obtained upon increasing the deposited Ni amount [cf. Figure 2e]. The area of NiO patches progressively extends with increasing the deposited amount, and 0.3 Å NiO (not shown) nearly fully cover the STO surface, with only little (4 × 1) structure visible in STM. LEED images acquired on the samples at different NiO coverages (not shown) do not exhibit any additional features in the diffraction pattern, but an overall increase of the inelastic background upon increasing the deposited material.

It is worth pointing out that a local distortion of the (4 × 1) rows is visible in STM in close proximity of the NiO patches. This is mostly evident wherever NiO patches extend up to the dark trenches separating adjacent dotted rows, as indicated by the white arrows in Figure 2c,d. In such regions the dark trenches appear wider in the in-plane direction, and a deeper corrugation (by 10−20 pm) is measured in STM.

Figure 2f shows the sample surface with 0.1 Å NiO postoxidized at 600 °C. The NiO patches coalesce into rectangular islands, and several defect structures are introduced in the STO substrate [orange solid lines in Figure 2f]. One type of defect appears as periodic, bright dots centered within the (4 × 1) structure. Another type of defect is a cross-shaped vacancy centered on one of the two rows of periodic dots, which build up the (4 × 1) structure. Finally, localized depressions occasionally appear next to NiO patches and possibly correspond to missing units of the surface structure. It should be mentioned that despite the relatively high temperature of 600 °C, only a small decrease (<6%) of the Ni 2p XPS intensity
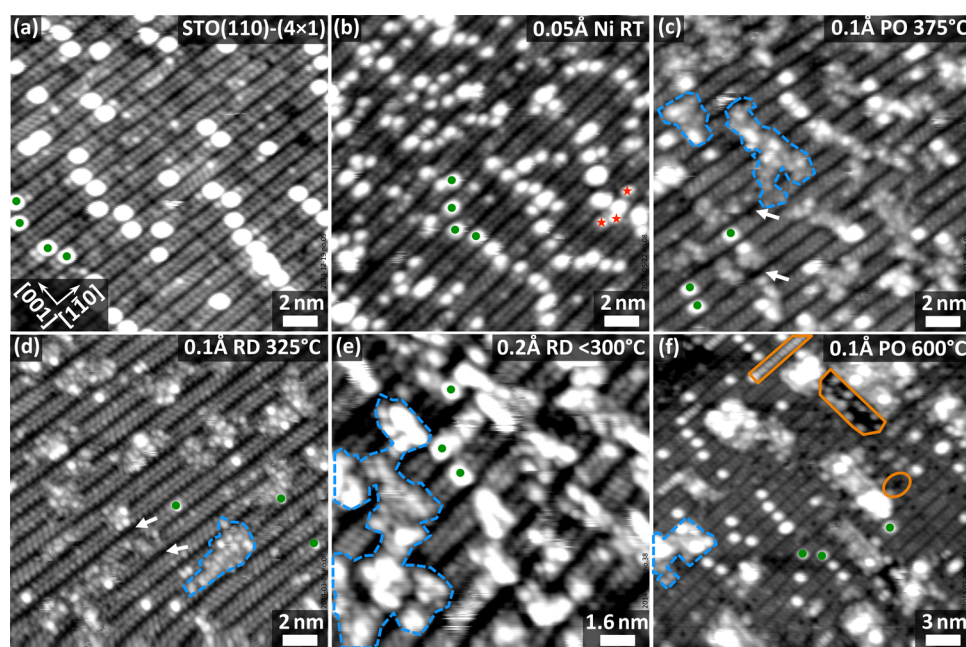
Figure 2. STM images [(a−d) 20 × 20 nm², (e) 16 × 16 nm², (f) 30 × 30 nm²] of differently treated SrTiO₃(110)-(4 × 1) surfaces. Green dots and red stars correspond to Sr and Ni adatoms, respectively. Dashed blue curves highlight selected NiO regions. Orange solid lines and white arrows indicate defects. (a) Pristine (4 × 1) surface. (b) Pristine surface after deposition of 0.05 Å Ni.[15] Panels c and d show 0.1 Å Ni postoxidized (PO) and reactively deposited (RD), respectively. (e) Reactively deposited 0.2 Å Ni. (f) 0.1 Å Ni after postoxidation at 600 °C. Tunneling parameters for panels a−f: U_S = +2.0 to +2.5 V, I_t = 0.02 to 0.3 nA.

was measured (not shown), excluding an extended intermixing of Ni atoms into the STO crystal.

XANES gives insight into the local electronic structure of the probed atoms. Electrons from occupied core levels get excited into unoccupied conduction band states, e.g., Ti 2p → Ti 3d transitions. As has been already pointed out, the (4 × 1) surface consists of tetrahedral TiO₄ units residing on bulk SrTiO₃ consisting of octahedral TiO₆ units. The spectral features corresponding to these two configurations can be disentangled in the XANES line shape, as has been recently shown [Wang et al., submitted]. The Ti 3d levels split into subsets with t_{2g}/e_g or t/e symmetry in an octahedral (Oh) or tetrahedral (Td) crystal field, respectively. Figure 3a shows XANES spectra of the Ti $L_{2,3}$ absorption edge for differently treated SrTiO₃(110) surfaces. Common to all spectra are a strong absorption peak at a photon energy of approximately 458 eV (Ti $2p_{3/2}$ → Ti 3d Oh-t_{2g}) followed by two overlapping peaks at 459 eV (Ti $2p_{3/2}$ → Ti 3d Td-e) and 460 eV (Ti $2p_{3/2}$ → Ti 3d Oh-e_g) and two broad overlapping features at 463 and 465 eV (Ti $2p_{1/2}$ → Ti 3d Oh-t_{2g} and Ti $2p_{1/2}$ → Ti 3d Oh-e_g).

Note the small shifts of the Ti $L_{2,3}$ peak at 458 eV for different treatments of the surface. These cannot be ascribed to band bending, which is caused by a local difference in electrostatic potential and should therefore affect all core levels and conduction band states equally. The shifts are therefore related to changes in the conduction band, i.e., in the Ti 3d levels. Overall, however, these shifts are below 0.2 eV. This indicates that the CBM is only minimally altered upon adsorption of NiO, as compared to the change in the VBM [see inset of Figure 1a].

A strong decrease of the tetrahedral signature after adsorption of Ni and NiO is visible in Figure 3a. This indicates that either the tetrahedral information is damped by the adsorbates or that the latter distort the TiO₄ tetrahedra. The latter possibility is consistent with the distortion, and disruption

of the surface structure, which was visible in STM after preparing a NiO-loaded surface at 300 °C [white arrows in Figure 2c,d] and 600 °C [Figure 2f], respectively. In general, Ti $L_{2,3}$ XANES spectra acquired in SEY mode (not shown) show the same absorption peaks as AEY with the relative peak ratios dominated by the octahedral coordination of Ti in bulk STO. Figure 3b shows the XANES spectrum of the O K edge. The spectrum appears similar for all surface treatments and acquisition modes (AEY and SEY), showing only minimal variations in the relative intensities of the main features. Because of the low signal, related to the small amounts of Ni deposited, the Ni $L_{2,3}$ XANES spectrum [Figure 3c] was acquired in secondary electron yield mode (see Materials and Methods section). Nevertheless, Ni atoms reside exclusively in the topmost surface layers. Therefore, the use of SEY mode is not limiting the surface sensitivity of the measurement. The photon energy at which adsorption at the L_3 edge occurs (approximately 853 eV) is consistent with previous reports for both metallic Ni and NiO samples.[20] In the case of postoxidized samples the main features of the characteristic line shape of NiO are observed. Namely, the intensity of the $L_{2,3}$ white lines with respect to the background is increased due to the oxidation of metallic Ni, resulting in an increased number of d holes for oxidized Ni species.[20]

H₂O Interaction with NiO-Modified STO(110)-(4 × 1). Here we studied the interaction of H₂O with the NiO-loaded SrTiO₃(110)-(4 × 1) surface by means of UPS/XPS and LEIS. The valence states of the adsorbed molecule allow distinguishing whether water is adsorbed molecularly or dissociatively. Molecularly adsorbed H₂O is characterized by its 1b1, 3a1, and 1b2 valence orbitals, with typical binding energies of 7, 10, and 14 eV, respectively.[21] On the other hand, OH species are characterized by their 1π (~6 eV) and 3σ (~11 eV) valence orbitals.[22]
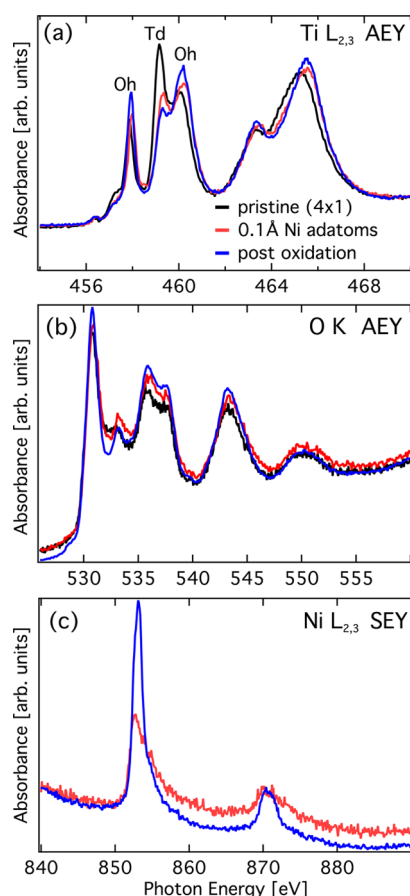
Figure 3. X-ray absorption spectra of the pristine surface, with 0.1 Å Ni adatoms, and after postoxidation to NiO (black, red, and blue curve, respectively). (a) Ti $L_{2,3}$ edge in Auger electron yield. Features related to Ti coordinated in tetrahedral or octahedral environment are indicated by Td and Oh, respectively. (b) O K edge in AEY. (c) Ni $L_{2,3}$ edge in secondary electrons yield.

Figure 4 shows valence band and O 1s core level photoemission spectra before (blue) and after (green) dosing
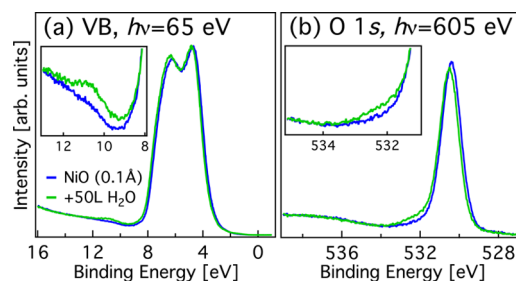

Figure 4. (a) Valence band and (b) O 1s photoemission spectra of NiO-loaded surfaces before (blue) and after (green) dosing 50 langmuirs of water at RT. The inset of (a) shows a zoom into the OH 3σ region (spectra aligned to the O 2s peak at 22 eV). Inset of (b) shows the O 1s high binding-energy region after aligning the spectra to the corresponding main peak.

50 langmuirs (1 langmuir = 1.33×10^{-6} mbar s) of H_2O on a (4×1) surface with 0.1 Å NiO. An increased density of states is found in regions commonly assigned to adsorbed OH, i.e., the OH 3σ state at 11 eV binding energy [see inset of Figure 4a, in which the spectra are aligned to the O 2s peak at $E_B \approx 22$ eV to highlight differences], and the high binding-energy

shoulder of the O 1s core-level [inset of Figure 4b, again with aligned O 1s peak energies]. After dosing 50 langmuirs of H_2O, the band bending decreased by 0.12 ± 0.15 eV.

A different approach for detecting adsorbed water is low-energy He$^+$ ion scattering (LEIS). LEIS is considered one of the most surface sensitive spectroscopic techniques with the ability of resolving small mass differences by choosing a suitable primary ion mass. Figure 5 shows ion scattering spectra of
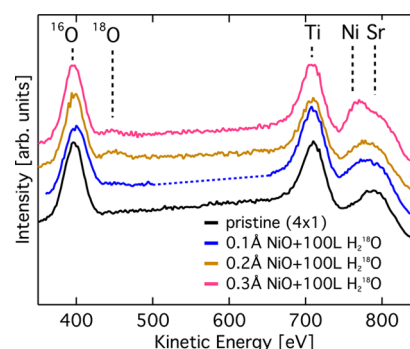

Figure 5. Low-energy He$^+$ ion scattering spectra acquired on the pristine SrTiO$_3$(110)-(4 × 1) and after depositing different amounts of NiO with subsequent dosing of 100 langmuirs of $H_2^{18}O$.

differently treated SrTiO$_3$(110)-(4 × 1) surfaces. The spectrum of the pristine (4 × 1) surface (black curve) shows peaks related to He$^+$ ions scattered at ^{16}O (∼400 eV), Ti (∼710 eV), and Sr (∼795 eV) atoms. It should be mentioned that upon impingement of 1000 eV He$^+$ ions a progressive degradation of the surface is observed, most likely due to intermixing of the first few surface layers. In particular, an inversion of the apparent Ti to Sr ratio is visible already after 15 scans (each scan takes about 1 min; the ion currents ranged from 15 to 23 nA, which translates into a total ion fluence of $(1.1-1.7) \times 10^{14}$ ions/cm^2 for each spectrum). In order to limit beam damage as much as possible while still retaining good statistics, we used only the sum of the first four scans for each LEIS spectrum in Figure 5. To investigate the adsorption of water on the NiO-loaded SrTiO$_3$(110)-(4 × 1) surface, we performed LEIS after dosing up to 100 langmuirs (1.3×10^{-7} mbar × 1000 s) of isotopically labeled water ($H_2^{18}O$). Dosing up to 100 langmuirs of $H_2^{18}O$ onto the pristine surface does not introduce any further features in the LEIS spectrum, consistent with the inert nature of this surface.[8]

We successively deposited increasing amounts of NiO onto the surface and subsequently dosed up to 100 langmuirs of $H_2^{18}O$, and each spectrum in Figure 5 corresponds to a freshly prepared sample. Nickel introduces a peak in LEIS spectra at a kinetic energy of approximately 770 eV. In addition, a peak at a kinetic energy of 450 eV is evolving. This peak is assigned to He$^+$ ions scattered at ^{18}O belonging to adsorbed water. The spectra acquired on samples with different amounts of NiO clearly show that water binds to the NiO-loaded surface, in agreement with the photoemission data in Figure 4. The existence of a larger ^{18}O peak in the case of 0.2 Å NiO compared to the case of 0.3 Å NiO (close to full coverage) possibly indicates that either H_2O adsorption or dissociation takes place at the NiO/SrTiO$_3$ boundary.

DISCUSSION

The combination of various spectroscopic techniques and direct-space imaging provides new insights into the NiO/STO system. UPS and XANES results indicate that the deposition of NiO onto the STO(110)-(4 × 1) surface effectively reduces the band gap of the system from 3.2 to approximately 1.7 eV. This change is visible in the altered onset of the valence band when NiO is present at the surface as well as in the relatively stable positions (within 0.2 eV) of Ti $L_{2,3}$ XANES peaks (probing the CBM) with and without NiO. Assuming that this VBM shoulder is hybridized with the O 2p valence band, these results suggest a considerable reduction of the band gap of the system NiO/STO, allowing harvesting of visible light (1.7 eV corresponding to 729 nm, i.e., near-infrared). Although the present data do not provide information on hybridization of these states, it is known from experiments with N-doped TiO_2 that such VBM shoulders can considerably enhance the visible-light response in photocatalysis experiments.[23] In addition, a pronounced (up to 0.8 eV) upward band bending is observed for the NiO-loaded surface. Photogenerated excitons can effectively dissociate in the electrostatic potential gradient related to the band bending, which drives electrons toward the bulk of the substrate and holes to the very surface, provided that extended states exist to allow charge transport before electron−hole recombination occurs. The excess holes located at the surface can then participate in the catalytic splitting of adsorbed H_2O.[24]

Combining STM and XANES, a disruption of the reconstructed surface lattice is observed upon adsorption of NiO. The resulting defects probably represent favorable adsorption sites for water, which is also consistent with ion scattering results. LEIS shows a higher water signal for the surface with 0.2 Å NiO compared to the nearly full coverage obtained upon depositing 0.3 Å NiO. This indicates that the adsorption may take place at the circumference of the NiO patches, i.e., at the triple phase boundary NiO/STO/UHV. No interdiffusion of Ni was detected; i.e., the two oxide phases are well separated. It should be mentioned that the patches observed in STM possibly consist of a mixed Ni−Ti oxide phase, since the amount of reactively deposited Ni resulting in a nearly full coverage (0.3 Å) approximately corresponds to 33% of a single NiO(110) layer. Such a mixed oxide phase might contribute to the damping of the tetrahedral feature in XANES.

In a previous study, we argued about the inertness of the pristine (4 × 1) surface to be caused by the undistorted tetrahedra forming the surface reconstruction.[8] Therefore, the distortion or disruption of these tetrahedra could be a reason for the enhanced reactivity of the surface toward water adsorption.

CONCLUSIONS

We have studied the morphology and electronic structure of the NiO-modified SrTiO₃(110)-(4 × 1) surface. An in-gap state, formed by the deposition of metallic Ni onto this surface, is transformed into a valence band shoulder upon oxidation of the Ni into NiO. This effectively increases the VBM with the CBM being unchanged, as seen in XANES, and therefore decreases the band gap of the system. Band bending is observed, which increases with the amount of NiO deposited. Furthermore, XANES results indicate that surface TiO_4 tetrahedra get considerably distorted or disrupted upon bonding with NiO, as is also evident from STM images of

NiO-covered surfaces. UPS and LEIS experiments confirm that the NiO activates the surface toward dissociative adsorption of H_2O, possibly involving sites at the interface between NiO patches and the substrate.

AUTHOR INFORMATION

Corresponding Authors
*(S.G.) E-mail gerhold@iap.tuwien.ac.at.
*(U.D.) E-mail diebold@iap.tuwien.ac.at; Tel +43-(0)1-58801-13425.
Notes
The authors declare no competing financial interest.

REFERENCES

(1) Sum, R.; Lang, H. P.; Güntherodt, H.-J. Scanning Force Microscopy Study of Single-Crystal Substrates Used for Thin-Film Growth of High-Temperature Superconductors. *Phys. C* **1995**, *242*, 174−182.

(2) Santander-Syro, A. F.; Copie, O.; Kondo, T.; Fortuna, F.; Pailhès, S.; Weht, R.; Qiu, X. G.; Bertran, F.; Nicolaou, A.; Taleb-Ibrahimi, A.; et al. Two-Dimensional Electron Gas with Universal Subbands at the Surface of SrTiO₃. *Nature* **2012**, *469*, 189−193.

(3) Wang, Z.; Zhong, Z.; Hao, X.; Gerhold, S.; Stöger, B.; Schmid, M.; Sanchez-Barriga, J.; Varykhalov, A.; Franchini, C.; Held, K.; et al. Anisotropic Two-Dimensional Electron Gas at SrTiO₃(110). *Proc. Natl. Acad. Sci. U. S. A.* **2014**, *111*, 3933.

(4) Mavroides, J. G.; Kafalas, J. A.; Kolesar, D. F. Photoelectrolysis of Water in Cells with SrTiO₃ Anodes. *Appl. Phys. Lett.* **1976**, *28*, 241−243.

(5) Fujishima, A.; Honda, K. Electrochemical Photolysis of Water at a Semiconductor Electrode. *Nature* **1972**, *238*, 37−38.

(6) Scaife, D. E. Oxide Semiconductors in Photoelectrochemical Conversion of Solar Energy. *Sol. Energy* **1980**, *25*, 41−54.

(7) Konta, R.; Ishii, T.; Kato, H.; Kudo, A. Photocatalytic Activities of Noble Metal Ion Doped SrTiO₃ Under Visible Light Irradiation. *J. Phys. Chem. B* **2004**, *108*, 8992−8995.

(8) Wang, Z.; Hao, X.; Gerhold, S.; Novotný, Z.; Franchini, C.; McDermott, E.; Schulte, K.; Schmid, M.; Diebold, U. Water Adsorption at the Tetrahedral Titania Surface Layer of SrTiO₃(110)-(4 × 1). *J. Phys. Chem. C* **2013**, *117*, 26060−26069.

(9) Enterkin, J. A.; Subramanian, A. K.; Russell, B. C.; Castell, M. R.; Poeppelmeier, K. R.; Marks, L. D. A Homologous Series of Structures on the Surface of SrTiO₃(110). *Nat. Mater.* **2010**, *9*, 245−248.

(10) Li, F.; Wang, Z.; Meng, S.; Sun, Y.; Yang, J.; Guo, Q.; Guo, J. Reversible Transition Between Thermodynamically Stable Phases with Low Density of Oxygen Vacancies on the SrTiO₃(110) Surface. *Phys. Rev. Lett.* **2011**, *107*, 036103.

(11) Townsend, T. K.; Browning, N. D.; Osterloh, F. E. Overall Photocatalytic Water Splitting with NiO_X−SrTiO₃ − A Revised Mechanism. *Energy Environ. Sci.* **2012**, *5*, 9543.

(12) Wang, Z.; Yang, F.; Zhang, Z.; Tang, Y.; Feng, J.; Wu, K.; Guo, Q.; Guo, J. Evolution of the Surface Structures on SrTiO₃(110) Tuned by Ti or Sr Concentration. *Phys. Rev. B: Condens. Matter Mater. Phys.* **2011**, *83*, 155453.

(13) Nyholm, R.; Andersen, J. N.; Johansson, U.; Jensen, B. N.; Lindau, I. Beamline I311 at MAX-LAB: a VUV/Soft X-Ray Undulator Beamline for High Resolution Electron Spectroscopy. *Nucl. Instrum. Methods Phys. Res., Sect. A* **2001**, *467−468*, 520−524.

(14) Cardona, M. Optical Properties and Band Structure of SrTiO₃ And BaTiO₃. *Phys. Rev.* **1965**, *140*, A651.

(15) Wang, Z.; Hao, X.; Gerhold, S.; Mares, P.; Wagner, M.; Bliem, R.; Schulte, K.; Schmid, M.; Franchini, C.; Diebold, U. Stabilizing

Single Ni Adatoms on a Two-Dimensional Porous Titania Overlayer at the SrTiO$_3$(110) Surface. *J. Phys. Chem. C* **2014**, *118*, 19904−19909.

(16) Greiner, M. T.; Helander, M. G.; Wang, Z.-B.; Tang, W.-M.; Lu, Z.-H. Effects of Processing Conditions on the Work Function and Energy-Level Alignment of NiO Thin Films. *J. Phys. Chem. C* **2010**, *114*, 19777−19781.

(17) Moulder, J. F.; Stickle, W. F.; Sobol, P. E.; Bomben, K. D. *Handbook of X-Ray Photoelectron Spectroscopy. A Reference Book of Standard Spectra for Identification and Interpretation of XPS Data*; Chastain, J., Ed.; Perkin-Elmer Corporation: Eden Prairie, MN, 1992.

(18) Diebold, U.; Pan, J. M.; Madey, T. E. Ultrathin Metal Film Growth on TiO$_2$(110): an Overview. *Surf. Sci.* **1995**, *331−333*, 845−854.

(19) Wang, Z.; Li, F.; Meng, S.; Zhang, J.; Plummer, E. W.; Diebold, U.; Guo, J. Strain-Induced Defect Superstructure on the SrTiO$_3$(110) Surface. *Phys. Rev. Lett.* **2013**, *111*, 056101.

(20) May, F.; Tischer, M.; Arvanitis, D.; Russo, M.; Dunn, J. H. Modifications of the Electronic and Magnetic Properties of Ultrathin Ni/Cu (100) Films Induced by Stepwise Oxidation. *Phys. Rev. B: Condens. Matter Mater. Phys.* **1996**, *53*, 1076−1079.

(21) Di Valentin, C.; Tilocca, A.; Selloni, A.; Beck, T. J.; Klust, A.; Batzill, M.; Losovyj, Y.; Diebold, U. Adsorption of Water on Reconstructed Rutile TiO$_2$(011)-(2 × 1): TiO Double Bonds and Surface Reactivity. *J. Am. Chem. Soc.* **2005**, *127*, 9895−9903.

(22) Thiel, P. A.; Madey, T. E. The Interaction of Water with Solid Surfaces: Fundamental Aspects. *Surf. Sci. Rep.* **1987**, *7*, 211−385.

(23) Tafen, D. N.; Wang, J.; Wu, N.; Lewis, J. P. Visible Light Photocatalytic Activity in Nitrogen-Doped TiO$_2$ Nanobelts. *Appl. Phys. Lett.* **2009**, *94*, 093101.

(24) Oberhofer, H.; Reuter, K. First-Principles Thermodynamic Screening Approach to Photo-Catalytic Water Splitting with Co-Catalysts. *J. Chem. Phys.* **2013**, *139*, 044710.